

The Equation of State of QCD up to very high temperatures

Matteo Bresciani,^{a,b,*} Michele Pepe,^{a,*} Mattia Dalla Brida^{a,b} and Leonardo Giusti^{a,b}

^aUniversity of Milano-Bicocca, Piazza della Scienza 3, Milan, I-20126, Italy

^bINFN Milano-Bicocca, Piazza della Scienza 3, Milan, I-20126, Italy

E-mail: m.bresciani9@campus.unimib.it, michele.pepe@mib.infn.it,
mattia.dallabrida@unimib.it, leonardo.giusti@unimib.it

We present the non-perturbative computation of the entropy density in QCD for temperatures ranging from 3 GeV up to the electro-weak scale, using $N_f = 3$ flavours of massless $O(a)$ -improved Wilson fermions. We adopt a new strategy designed to be computationally efficient and based on formulating thermal QCD in a moving reference frame, where the fields satisfy shifted boundary conditions in the temporal direction and periodic boundary conditions along the spatial ones. In this setup the entropy density can be computed as the derivative of the free-energy density with respect to the shift parameter. For each physical temperature, we perform Monte Carlo simulations at four values of the lattice spacing in order to extrapolate the numerical data of the entropy density to the continuum limit. We achieve a final accuracy of approximately 0.5-1.0% and our results are compared with predictions from high-temperature perturbation theory.

The 41st International Symposium on Lattice Field Theory (LATTICE2024)
28 July - 3 August 2024
Liverpool, UK

*Speakers

1. Introduction

There is significant interest from particle physics to cosmology in understanding the thermodynamic properties of the high temperature regime of QCD. In particular, the Equation of State (EoS) at all temperatures up to the electro-weak scale is crucial theoretical input for cosmological models that describe the early evolution of the Universe. For instance, it is believed that the EoS played a key role in shaping the spectrum of primordial gravitational waves and determining the abundance of several dark matter candidates, such as WIMPs and/or axions [1, 2]. In particle physics, the EoS is required in the analysis of data coming from heavy-ion colliders and for the study of QCD under extreme conditions.

The EoS has been determined from non-perturbative lattice calculations up to temperatures of about 1 GeV in various staggered quark setups [3–6], with a precision of a few percent. Beyond this range, it is known only from perturbative computations resummed using thermal effective theories of QCD [7, 8] and from hard-thermal-loop perturbation theory [9, 10], which rely on small values of the running coupling constant holding at asymptotically high temperatures. However, the perturbative expansion suffers from poor convergence, leading to an unsatisfactory description of the thermodynamic features of quarks and gluons up to the electro-weak scale [11–13].

In these Proceedings we present the results of Ref. [14] on the non-perturbative determination of the QCD EoS with a precision of about 0.5-1.0% in the unexplored range of temperatures between 3 and 165 GeV. We carried out the calculation by numerical simulations with $N_f = 3$ massless flavours of $O(a)$ -improved Wilson fermions. This result is achieved through a new strategy based on two key novelties. First, instead of using a hadronic scheme, we determine the lines of constant physics by imposing that a renormalized coupling, defined non-perturbatively in a finite volume scheme, assumes a prescribed value [12]. Second, we consider the setup of thermal QCD in a moving reference frame, which allows for the direct computation of the entropy density by exploiting the (Euclidean) Lorentz invariance of the theory [15]. In particular, this approach prevents the need of the zero-temperature subtraction usually required for the definition of thermodynamic potentials. The combination of these elements allows us to overcome the window problem that arises when simulating a high-energy scale and a low-energy one at the same lattice spacing: in our case, the temperature and the hadronic scale, respectively. This strategy makes the high-temperature regime accessible to non-perturbative lattice studies with controlled systematic effects and affordable computational effort. It has already proved successful for the non-perturbative determination of the EoS of SU(3) Yang-Mills theory [11] and, more recently, of the screening spectrum of QCD [12, 13] up to very high temperatures.

2. EoS from QCD in a moving reference frame

The SO(4) Euclidean invariance of QCD in the continuum allows us to define the thermal theory in a moving reference frame. In the path integral formalism, this corresponds to introducing a spatial shift $\xi = (\xi_1, \xi_2, \xi_3)$ when closing the boundary conditions of the gauge field, A_μ , and of

T	$\bar{g}_{\text{SF}}^2(\mu = T\sqrt{2})$	T (GeV)
T_0	1.01636	164.6(5.6)
T_1	1.11000	82.3(2.8)
T_2	1.18446	51.4(1.7)
T_3	1.26569	32.8(1.0)
T_4	1.3627	20.63(63)
T_5	1.4808	12.77(37)
T_6	1.6173	8.03(22)
T_7	1.7943	4.91(13)
T_8	2.0120	3.040(78)

Table 1: Values of the Schrödinger functional coupling in $N_f = 3$ QCD with Wilson action used to renormalize the bare parameters at the physical temperatures considered in this work, reported in the last column.

the fermionic fields, ψ and $\bar{\psi}$, along the compact direction of length L_0 [15, 16]:

$$\begin{aligned}
A_\mu(x_0 + L_0, \mathbf{x}) &= A_\mu(x_0, \mathbf{x} - L_0\xi), \\
\psi(x_0 + L_0, \mathbf{x}) &= -\psi(x_0, \mathbf{x} - L_0\xi), \\
\bar{\psi}(x_0 + L_0, \mathbf{x}) &= -\bar{\psi}(x_0, \mathbf{x} - L_0\xi).
\end{aligned} \tag{1}$$

Periodic boundary conditions can be set in the other directions, taken of length L . In the presence of shifted boundary conditions [15], the thermal system has spatial size $V_s = L^3/\sqrt{1 + \xi^2}$ and it is at the temperature $T^{-1} = L_0\sqrt{1 + \xi^2}$. The free-energy density of the thermal system is related as usual to the partition function \mathcal{Z} ,

$$f_\xi = -\frac{T}{V_s} \ln \mathcal{Z} = -\frac{1}{L_0 L^3} \ln \mathcal{Z}, \quad \mathcal{Z} = \int DAD\bar{\psi}D\psi e^{-S}, \tag{2}$$

where S is the QCD action. Taking into account that, in the framework of shifted boundary conditions, the temperature can be changed by varying ξ at fixed L_0 and that the pressure $p = -f_\xi$, we obtain the following equation [15]

$$\frac{s}{T^3} = \frac{1 + \xi^2}{\xi_k} \frac{1}{T^4} \frac{\partial f_\xi}{\partial \xi_k} \tag{3}$$

which relates the entropy density $s = dp/dT$ to the derivative of the free-energy density f_ξ with respect to the shift. The power divergence resulting from the mixing of the free energy with the identity is removed by the derivative in the shift and the entropy defined in Eq. (3) is directly a physical quantity. The pressure $p(T)$ can then be obtained by integrating the entropy in the temperature, while the energy density $e(T)$ follows from the relation $Ts = e + p$.

3. Lattice setup and renormalization

The QCD action on the lattice, $S = S_G + S_F$, is given by the sum of a gluonic and a fermionic component. The gluonic part, S_G , involves only the gauge field and we consider the Wilson

plaquette action

$$S_G = \frac{6}{g_0^2} \sum_x \sum_{\mu < \nu} \left[1 - \frac{1}{3} \text{Tr} \{ U_{\mu\nu}(x) \} \right], \quad (4)$$

where the trace is over the colour index, g_0 is the bare gauge coupling and $\mu, \nu = 0, 1, 2, 3$. The plaquette field $U_{\mu\nu}$ is defined as

$$U_{\mu\nu}(x) = U_\mu(x) U_\nu(x + a\hat{\mu}) U_\mu^\dagger(x + a\hat{\nu}) U_\nu^\dagger(x) \quad (5)$$

where $U_\mu(x) \in \text{SU}(3)$ is the link field. The fermionic part S_F reads

$$S_F = a^4 \sum_x \bar{\psi}(x) (D + m_0) \psi(x), \quad (6)$$

where D is the $O(a)$ -improved Wilson-Dirac operator and m_0 is the bare quark mass. On the lattice, the link field and the fermionic fields satisfy shifted boundary conditions analogous to the ones in Eq. (1), with the field A_μ replaced by U_μ . The fields are periodic along the spatial directions.

In QCD with $N_f = 3$, the non-perturbative running of the Schrödinger functional coupling \bar{g}_{SF}^2 is known precisely in the continuum limit [17–19]. Building on this result, we determine the lines of constant physics at a given temperature T by fixing the value of the renormalized coupling at finite lattice spacing to match its value in the continuum at a scale $\mu = T\sqrt{2}$:

$$\bar{g}_{\text{SF}}^2(g_0^2, a\mu) = \bar{g}_{\text{SF}}^2(\mu), \quad a\mu \ll 1. \quad (7)$$

This condition fixes the dependence of the bare coupling g_0 on the lattice spacing, for values of a at which the scale μ and therefore the temperature can be easily accommodated. As a consequence, each temperature can be simulated at several lattice resolutions and the continuum limit can be taken with confidence. In this study we have considered 9 values of temperature between 3 GeV and 165 GeV, as reported in Table 1. The critical mass m_{cr} at given bare parameters is then defined by requiring the PCAC mass to vanish in the Schrödinger functional setup. We refer to Appendix B and to Table 4 of [12] for the technical details and for the resulting lines of constant physics.

4. Entropy density on the lattice

As discussed in Section 2, the entropy density defined in Eq. (3) is directly a physical quantity. This allows us to discretize the equation on the lattice and to determine the entropy density by extrapolating to the continuum limit the measurements obtained from Monte Carlo simulations performed at various lattice spacings, all corresponding to the same fixed physical temperature T . Thus, at given values of L_0/a and g_0^2 , we have

$$\frac{s}{T^3} = \frac{1 + \xi^2}{\xi_k} \frac{1}{T^4} \frac{\Delta f_\xi}{\Delta \xi_k}, \quad (8)$$

where

$$\frac{\Delta f_\xi}{\Delta \xi_k} = \frac{L_0}{4a} \left(f_{\xi + \frac{2a}{L_0} \hat{k}} - f_{\xi - \frac{2a}{L_0} \hat{k}} \right) \quad (9)$$

is the 2-point discrete symmetric derivative of the free-energy with respect to the k -th component of the shift ¹. For computational efficiency, at fixed L_0/a and g_0^2 the discrete derivative of the free-energy density is conveniently decomposed into two contributions,

$$\frac{\Delta f_\xi}{\Delta \xi_k} = \frac{\Delta(f_\xi - f_\xi^\infty)}{\Delta \xi_k} + \frac{\Delta f_\xi^\infty}{\Delta \xi_k}, \quad (10)$$

where f_ξ^∞ is the free-energy density of QCD with infinitely massive quarks, i.e. in the static limit. The first term can be rewritten as

$$\frac{\Delta(f_\xi - f_\xi^\infty)}{\Delta \xi_k} = -\frac{\Delta}{\Delta \xi_k} \int_0^\infty dm_q \frac{\partial f_\xi^{m_q}}{\partial m_q} = -\int_0^\infty dm_q \frac{\Delta \langle \bar{\psi} \psi \rangle_\xi^{m_q}}{\Delta \xi_k}, \quad (11)$$

where $m_q = m_0 - m_{\text{cr}}(g_0^2, L_0)$ is the bare subtracted quark mass. The discrete derivative of the chiral condensate $\langle \bar{\psi} \psi \rangle_\xi$ with respect to the shift is defined similarly to Eq. (9). The second term in Eq. (10) is evaluated in the static quark limit of QCD. We rewrite it as follows,

$$\frac{\Delta f_\xi^\infty}{\Delta \xi_k} = \frac{\Delta f_\xi^{\infty,(0)}}{\Delta \xi_k} + g_0^2 \frac{\Delta f_\xi^{\infty,(1)}}{\Delta \xi_k} - \int_0^{g_0^2} du \left(\frac{1}{u} \frac{\Delta \langle S_G \rangle_\xi^\infty}{\Delta \xi_k} \Big|_{g_0^2=u} + \frac{\Delta f_\xi^{\infty,(1)}}{\Delta \xi_k} \right), \quad (12)$$

where $f_\xi^{\infty,(0)}$ and $f_\xi^{\infty,(1)}$ represent, respectively, the tree-level and one-loop coefficients of the perturbative expansion on the lattice of the free-energy density in pure gauge theory.

In the following we discuss the numerical evaluation on the lattice of the two contributions in Eqs. (11) and (12). We consider four resolutions $L_0/a = 4, 6, 8, 10$ of the compact direction, while the three spatial directions are taken to be of the same size, equal to $L/a = 144$. Finite volume effects are exponentially suppressed as $e^{-M_{\text{gap}}L}$ for $L \rightarrow \infty$, where M_{gap} is the mass gap of the theory. In the high-temperature regime that we are investigating, we have $M_{\text{gap}} \propto T$ with a coefficient close to unity [12, 15], and therefore we expect finite size effects to be well below the statistical accuracy of our numerical results. We choose the shift vector $\xi = (1, 0, 0)$ as it turned out to lead to milder discretization effects in perturbation theory and in other studies employing shifted boundary conditions [12, 20, 21].

4.1 Integration in the bare mass

In this subsection we discuss the method we have used to compute the integral in the bare subtracted quark mass appearing in Eq. (11). At given values of L_0/a and g_0^2 , we split the integration interval into three domains. The first one, corresponding to $m_q/T \in [0, 5]$, gives the largest contribution to the integral and it is computed with a 10-point Gaussian quadrature. The second interval, where we go up to $m_q/T = 20$ ($m_q/T = 35$ for $L_0/a = 4$), is computed with a 7-point Gaussian quadrature and gives about 20% of the result. Finally, the last interval comes from the asymptotic tail $m_q/T \rightarrow \infty$ and contributes to the total by two standard deviations at most. It is estimated with a 3-point Gaussian quadrature, after a change of variable to the hopping parameter $\kappa = 1/(2am_0 + 8)$ which leads to a compact integration interval. This combination of Gaussian quadratures has been chosen and optimized by using perturbation theory as guidance so as to keep

¹We use the two-point discrete derivative due to constraints related to the simulation software.

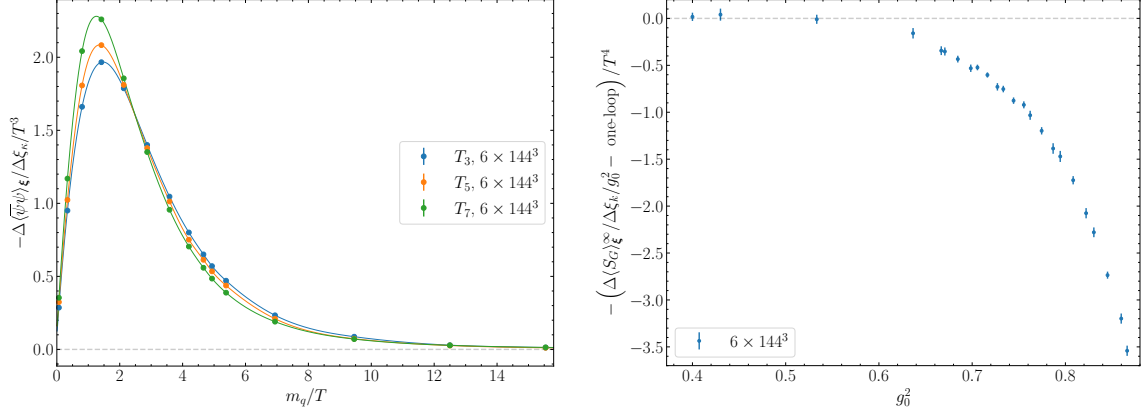


Figure 1: Left: Derivative in the shift of the chiral condensate as a function of m_q/T at some selected bare parameters. Points have been interpolated with a cubic spline to guide the eye. Error bars are smaller than the markers. Right: Derivative in the shift of the pure gauge action as a function of g_0^2 for $L_0/a = 6$. For convenience we subtracted from the data the result at one-loop order in lattice perturbation theory.

the systematic error coming from the numerical integration well below the statistical accuracy of the numerical results.

The computation of the discrete derivative in the integrand of Eq. (11) requires performing two Monte Carlo simulations to measure the chiral condensate at the two shifts $\xi = (1 \pm 2a/L_0, 0, 0)$. By carrying out this calculation for all the bare mass values determined by the Gaussian quadratures, we obtain a total of 40 independent simulations for each given value of L_0/a and g_0^2 . The left panel of Figure 1 shows the resulting integrand function for a selection of bare parameters. The final accuracy on the integral ranges from a few permille for $L_0/a = 4$ to about 1% for $L_0/a = 10$.

4.2 Integration in the bare coupling

The computation of the integral in Eq. (12) is carried out in SU(3) Yang-Mills theory. Although this contribution has larger variance compared to the one in Eq. (11), pure gauge simulations are significantly less computationally demanding and high precision can be reached with a moderate effort. For a given value L_0/a , let $g_0^2|_{T_i}$ be the value of the bare coupling determined from the lines of constant physics at temperature T_i with $i = 0, 1, \dots, 8$. The observable we have to integrate is $\Delta\langle S_G\rangle_{\xi}^{\infty}/\Delta\xi_k$ and we split the integration interval $[0, g_0^2|_{T_i}]$ into several parts combining different integration schemes.

In the domain $g_0^2 \in [0, 6/15]$ the integral is computed with a 2-point trapezoidal rule (3-point Simpson rule for $L_0/a = 4$). The interval $g_0^2 \in [6/15, 6/9]$ is integrated with a 3-point Gaussian quadrature. For the resolutions $L_0/a = 4, 6$, the domain $g_0^2 \in [6/9, g_0^2|_{T_0}]$ is integrated with a 3-point Gaussian quadrature for $L_0/a = 4$ and with the midpoint rule for $L_0/a = 6$. The interval $g_0^2 \in [6/9, g_0^2|_{T_1}]$ is computed with a 3-point Gaussian quadrature. At the lower temperatures T_i , $i > 1$, the value of the integral is obtained by adding to the T_{i-1} result the integral in the segment $g_0^2 \in [g_0^2|_{T_{i-1}}, g_0^2|_{T_i}]$, estimated with a 3-point Gaussian quadrature for $i = 2, 3, 4, 5, 6$, and a 5-point Gaussian quadrature for $i = 7, 8$.

Similarly to the fermionic case, the computation of the discrete derivative $\Delta\langle S_G\rangle_{\xi}^{\infty}/\Delta\xi_k$ requires performing two Monte Carlo simulations to measure $\langle S_G\rangle_{\xi}^{\infty}$ at the two shifts $\xi = (1 \pm 2a/L_0, 0, 0)$.

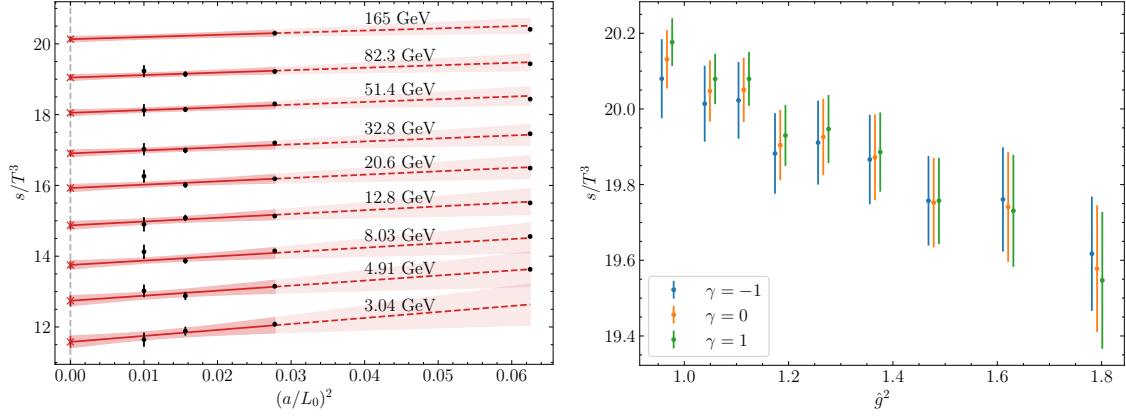


Figure 2: Left: The black points are the values of s/T^3 at fixed lattice spacing a/L_0 and given temperature. Points at temperature T_n have been shifted downward by n for better readability. The red bands represent our best fit to the continuum limit. Right: Effect of logarithmic corrections on the continuum extrapolated values of the best fit, see main text for details.

This leads to a total of 74 independent simulations for $L_0/a = 4$, 68 for $L_0/a = 6$ and 66 for $L_0/a = 8, 10$. The pure gauge ensembles for this computation have been generated in Monte Carlo simulations where the basic sweep is a combination of heatbath and overrelaxation [22] updates of the link variables, using the Cabibbo–Marinari scheme [23]. The right panel of Figure 1 shows a representative case for the integrand function in g_0^2 . At each temperature, the accuracy on the integral is $\sim 0.5\%$ for $L_0/a = 4, 6$, $\sim 1\%$ for $L_0/a = 8$ and $\sim 1.5\%$ for $L_0/a = 10$.

4.3 Continuum limit

In this subsection we discuss the extrapolation to the continuum limit of the results for the entropy density we have obtained by Monte Carlo simulations. At all orders in the lattice spacing, discretization effects of order $O(g^0)$ and $O(g^2)$ can be removed by improving the observable at one-loop order. This can be accomplished, for instance, considering

$$s(L_0/a, g_0^2) \rightarrow s(L_0/a, g_0^2) \frac{s_0 + s_2 \cdot \left(\frac{g}{2\pi}\right)^2}{s_0(L_0/a) + s_2(L_0/a) \cdot \left(\frac{g}{2\pi}\right)^2} \quad (13)$$

where $g^2 \equiv \bar{g}_{\text{SF}}^2(1/L_0)$ while $s_0(L_0/a)$ and $s_2(L_0/a)$ are the tree-level and the one-loop coefficients computed in lattice perturbation theory in the thermodynamic limit. Their values for the relevant L_0/a are listed in Table 2, together with the results in the continuum limit. After performing this one-loop improvement of the lattice results, the leading discretization effects are expected to be of $O(g^3 a^2)$. On general grounds, at finite temperature, we expect also odd powers in the coupling to be present.

We computed the entropy density in the continuum by extrapolating the one-loop improved lattice entropy density using a combined fit of the data collected at the various temperatures. We have considered the following fit function,

$$s(T_i, a/L_0)/T_i^3 = s(T_i)/T_i^3 + d_2 \left(\frac{a}{L_0}\right)^2 g_i^3 + d_3 \left(\frac{a}{L_0}\right)^3 g_i^3 \quad (14)$$

L_0/a	4	6	8	10	∞
s_0	4.719	3.438	3.145	3.059	2.969
s_2	-23.465	-13.085	-9.955	-9.089	-8.438

Table 2: Coefficients for the one-loop improvement of the lattice entropy density.

where $i = 0, \dots, 8$ and $g_i \equiv \bar{g}_{\text{SF}}(\sqrt{2}T_i)$. The fit parameters $s(T_i)$ represent the continuum values at fixed temperature T_i , and the coefficients d_2, d_3 parametrize the discretization effects. We first fitted data with $L_0/a = 4, 6, 8, 10$ by setting either $d_3 = 0$ or $d_3 \neq 0$. While both fits have $\chi^2/\chi_{\text{exp}}^2 \approx 1$, with χ_{exp} defined as in Ref. [24], the former gives values for $s(T_i)$ with errors 3-4 times smaller. Although compatible within the larger errors of the second fit, the extrapolated central values of the first fit are systematically higher.

A quadratic fit of the lattice artifacts ($d_3 = 0$), excluding the data at $L_0/a = 4$, yields $\chi^2/\chi_{\text{exp}}^2 \approx 0.7$. This fit provides estimates of the continuum values $s(T_i)$ that are in good agreement with those obtained from the full dataset and the $d_3 \neq 0$ fit, both in terms of central values and error size. This suggests that the data at $L_0/a = 4$ are likely affected by discretization effects of higher order than a^2 . Thus, we used the data at the coarsest lattice spacing only to estimate the size of the $O(a^3)$ contributions and included these as a systematic error of the points at finer lattice spacing.

More specifically, we used the value of d_3 obtained from the fit of the full dataset as an estimate of the systematic uncertainty and we added it in quadrature to the statistical errors, $\sigma(T_i, a/L_0)$, of the normalized entropy density at given temperature and lattice spacing

$$\sigma^2(T_i, a/L_0) \rightarrow \sigma^2(T_i, a/L_0) + [d_3(a/L_0)^3 g_i^3]^2. \quad (15)$$

This quantity receives contributions from the statistical variance of the Monte Carlo ensembles, from the uncertainties related to the definition of the lines of constant physics [12, 18] (although negligible with respect to the total), and from the correlations introduced by the integration in the bare coupling, see Eq. (12). All the correlations have been properly taken into account using the tools of Refs. [25, 26].

The final best fit is the one considering data with $L_0/a > 4$, $d_3 = 0$ in the fit ansatz Eq. (14), and errors as in Eq. (15) for the definition of the weights in the χ^2 -function minimized by the fit. The resulting values for $s(T_i)/T_i^3$ are reported in Table 3, and have a relative error of 0.5-1.0%.

We performed several checks to further corroborate the robustness of our best fit. The continuum results are stable against adding a term like $(a/L_0)^2 g_i^4$ to Eq. (14). Furthermore, we repeated the whole analysis replacing $d_3(a/L_0)^3 g_i^3$ with $d_4(a/L_0)^4 g_i^3$ in the fit ansatz. We obtain perfectly compatible results for the $s(T_i)$ with errors that are 10-20% smaller. Similar conclusions hold when replacing $g_i^3 \rightarrow g_i^4$ in both a^2 and a^3 terms. Finally, we also checked the impact of logarithmic corrections to the leading discretization effects, of $O(a^2)$, using the modified fit function [27–29]

$$s(T_i, a/L_0)/T_i^3 = s(T_i)/T_i + d_2 [\bar{g}_{\text{SF}}^2(\pi/a)]^\gamma \left(\frac{a}{L_0}\right)^2 g_i^2. \quad (16)$$

The results for $s(T_i)$ change by less than 1 standard deviation with respect to the best fit, $\gamma = 0$, when the effective anomalous dimension is varied in the interval $\gamma \in [-1, 1]$. The comparison for three selected values is shown in the right panel of Figure 2.

T	T (GeV)	s/T^3
T_0	165(6)	20.13(8)
T_1	82.3(2.8)	20.05(8)
T_2	51.4(1.7)	20.05(9)
T_3	32.8(1.0)	19.90(9)
T_4	20.6(6)	19.93(10)
T_5	12.8(4)	19.87(11)
T_6	8.03(22)	19.75(12)
T_7	4.91(13)	19.74(15)
T_8	3.04(8)	19.58(17)

Table 3: Continuum extrapolated results for the normalized entropy density s/T^3 at the 9 temperatures considered in this study.

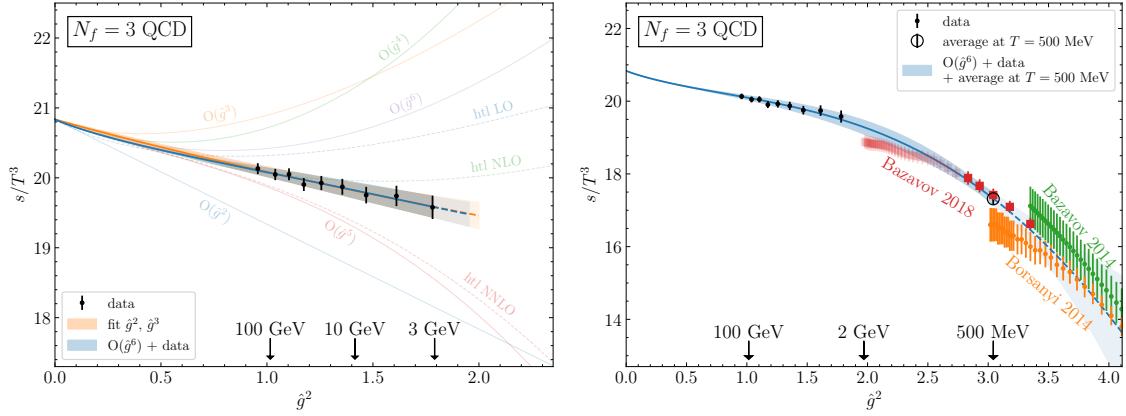


Figure 3: Left: Normalized entropy density s/T^3 in the continuum limit as a function of $\hat{g}^2(T)$. The shadowed curves represent the perturbative value up to the indicated order, and the prediction from hard-thermal-loop (htl) [9, 10]. The orange and blue bands (grey when the two overlap) correspond to the fits to Eqs. (18) and (19), see main text for the details. Right: s/T^3 as a function of $\hat{g}^2(T)$. The black points are our continuum values. At lower temperatures results from the literature are also shown, labelled as “Borsanyi 2014” [3], “Bazavov 2014” [4] and “Bazavov 2018” [5]. The black circle marker is the weighted average of these results at $T = 500$ MeV. Finally, the blue band is our best parametrization of s/T^3 for $N_f = 3$ QCD at $T \geq 500$ MeV.

5. Discussion

We parametrize the temperature dependence of the continuum extrapolated entropy density through the function $\hat{g}^2(T)$, defined as the 5-loop strong coupling in the $\overline{\text{MS}}$ scheme [30] renormalized at the scale $2\pi T$. Its leading order expression reads

$$\frac{1}{\hat{g}^2(T)} = \frac{9}{8\pi^2} \ln \frac{2\pi T}{\Lambda_{\overline{\text{MS}}}} + \dots, \quad (17)$$

where the value of the Lambda parameter is $\Lambda_{\overline{\text{MS}}} = 341$ MeV [19]. For our purposes this is only a convenient choice which makes simpler to compare the non-perturbative results with the prediction

of perturbation theory. In left panel of Figure 3 we plot the continuum results of the entropy density reported in Table 3 as a function of \hat{g}^2 .

A simple parametrization is a polynomial in \hat{g} of the form

$$\frac{s}{T^3} = \frac{32\pi^2}{45} \left[s_0 + s_2 \left(\frac{\hat{g}}{2\pi} \right)^2 + s_3 \left(\frac{\hat{g}}{2\pi} \right)^3 \right]. \quad (18)$$

We first set $s_3 = 0$ taking s_0 and s_2 as fit parameters. The resulting values are $s_0 = 2.954(15)$ and $s_2 = -3.6(7)$: notably, the former is in agreement within 1 standard deviation with the Stefan-Boltzmann (SB) value $s_0^{\text{SB}} = 2.969$, obtained in the infinite temperature limit. We thus fit our results enforcing $s_0 = s_0^{\text{SB}}$ in Eq. (18) and leaving s_2, s_3 as fit parameters. The resulting coefficients are $s_2 = -5.1(9)$, $s_3 = 5(5)$ and this fit is represented as the orange band in the left panel of Figure 3. Thus, a simple, third-order polynomial in \hat{g} is sufficient for the description of the entropy density in the interval of temperatures considered in this study, which spans almost two orders of magnitude. However, we also point out that the slope in \hat{g}^2 resulting from that fit differs from the perturbative prediction -8.438 by a few standard deviations.

It is interesting to compare our non-perturbative results with the expectations coming from perturbative computations performed at high temperatures. We thus consider a fit function with all the known perturbative coefficients,

$$\frac{s}{T^3} = \frac{32\pi^2}{45} \left[\sum_{k=0}^6 s_k \left(\frac{\hat{g}}{2\pi} \right)^k + q_c \left(\frac{\hat{g}}{2\pi} \right)^6 + s_7 \left(\frac{\hat{g}}{2\pi} \right)^7 \right], \quad (19)$$

where s_0, \dots, s_6 are obtained from the perturbative expansion of the pressure [8]. The fit function (19) is thus expected to reproduce the correct behaviour at asymptotically high temperatures. We have two fit parameters: q_c represents the unknown contributions at order $\mathcal{O}(\hat{g}^6)$ including those from the non-perturbative ultrasoft modes, and s_7 takes into account higher order effects in the weak coupling expansion. By fitting our data we obtain $q_c = -5.1(1.7) \cdot 10^3$, $s_7 = 1.3(7) \cdot 10^4$ with $\chi^2/\chi_{\text{exp}}^2 = 0.58$. The corresponding curve is displayed in blue in the left panel of Figure 3. The two fits Eq. (18) with the SB value enforced, and Eq. (19) are in very good agreement in the interval of temperatures considered in this study, and also for $T \rightarrow \infty$.

For temperatures up to about 500 MeV, the EoS of $N_f = 2 + 1$ QCD has been computed in the continuum limit by the Wuppertal-Budapest collaboration [3] and by the HotQCD collaboration [4, 5]. Since the contribution of the light quark masses at $T = 500$ MeV is negligible within the statistical accuracy quoted by the two collaborations [31], we can compare these results with ours.

Including in the fit of Eq. (19) the value $s/T^3 = 17.31(16)$ at $T = 500$ MeV, obtained from the average of the results of the two collaborations, the resulting fit parameters are $q_c = -4.0(1.1) \cdot 10^3$, $s_7 = 7(4) \cdot 10^3$ with $\chi^2/\chi_{\text{exp}}^2 = 0.79$. This is our best parametrization of the normalized entropy density of $N_f = 3$ QCD for $T \geq 500$ MeV, and it is represented as the blue shadowed curve in the right panel of Figure 3. The relative error is $\lesssim 1\%$ in the whole temperature range considered.

Following Ref. [8], the pressure can be parameterized analogously to Eq. (19) with $p_7 = s_7 + (5b_0p_5 + 3b_1p_3)/4$, where $b_0 = 9/4$, $b_1 = 4$, and p_3 and p_5 are given in Ref. [8]. The energy density is then determined using the relation $e = Ts - p$.

6. Conclusions

In a recent publication [14], and in these Proceedings, we show the first non-perturbative computation of the EoS of QCD with $N_f = 3$ massless flavours, in the range of temperatures from 3 to 165 GeV. The final accuracy on our primary observable, the entropy density, is 0.5-1.0% and is dominated by the statistical error. By combining our data with non-perturbative results at $T = 500$ MeV from the literature and by enforcing the behaviour at asymptotically high temperatures using the known perturbative expansion, we could determine the temperature dependence of the entropy density for $T \geq 500$ MeV with a relative error of at most $\sim 1\%$. The pressure and the energy density can then be computed as well using standard thermodynamic relations [14].

This result relies on a completely new strategy, based on two pillars: on the one hand, we determine the lines of constant physics at very high temperature by imposing the renormalization conditions through the non-perturbatively defined strong coupling \bar{g}_{SF}^2 of QCD, whose running in the continuum is known with high accuracy [19]. This gives us the freedom to choose the renormalization scales, at which the bare parameters are renormalized, to be close to the temperatures simulated [12]. On the other hand, we formulate QCD in a moving reference frame [15, 32] which represents a convenient setup where thermodynamic potentials can be determined without the need of any zero-temperature subtraction.

Our strategy can be readily generalized to the case of QCD with four or five (massive) flavours. This result would directly improve the present knowledge of the Standard Model EoS, whose uncertainty for temperatures from a few GeV up to the electro-weak scale is dominated by the systematics introduced by the poor convergence of the perturbative expansion of the QCD component [1, 2].

Finally, we also notice that in the presence of shifted boundary conditions the EoS can be accessed through suitable one-point functions of the Energy-Momentum tensor (EMT) [15]. On the lattice, this gives us the handle to compute in a non-perturbative way the renormalization constants that define the lattice EMT. Some preliminary results for the renormalization factors of the non-singlet components with a precision of a few percent are reported in Ref. [33]. This is a notoriously challenging theoretical problem in lattice QCD [34–37], whose solution would open the way to further first-principle investigations of the thermal properties of QCD through the correlation functions of the (renormalized) EMT [38].

Acknowledgments

We acknowledge PRACE for awarding us access to the HPC system MareNostrum4 at the Barcelona Supercomputing Center (Proposals n. 2018194651 and 2021240051) where some of the numerical results presented in this letter have been obtained. We also thank CINECA for providing us with a very generous access to Leonardo during the early phases of operations of the machine and for the computer time allocated via the CINECA-INFN, CINECA-Bicocca agreements. The R&D has been carried out on the PC clusters Wilson and Knuth at Milano-Bicocca. We thank all these institutions for the technical support. This work is (partially) supported by ICSC – Centro Nazionale di Ricerca in High Performance Computing, Big Data and Quantum Computing, funded by European Union – NextGenerationEU.

References

- [1] K. Saikawa and S. Shirai, *Primordial gravitational waves, precisely: The role of thermodynamics in the Standard Model*, *JCAP* **05** (2018) 035 [[1803.01038](#)].
- [2] K. Saikawa and S. Shirai, *Precise WIMP Dark Matter Abundance and Standard Model Thermodynamics*, *JCAP* **08** (2020) 011 [[2005.03544](#)].
- [3] S. Borsanyi, Z. Fodor, C. Hoelbling, S.D. Katz, S. Krieg and K.K. Szabo, *Full result for the QCD equation of state with 2+1 flavors*, *Phys. Lett. B* **730** (2014) 99 [[1309.5258](#)].
- [4] HotQCD collaboration, *Equation of state in (2+1)-flavor QCD*, *Phys. Rev. D* **90** (2014) 094503 [[1407.6387](#)].
- [5] A. Bazavov, P. Petreczky and J.H. Weber, *Equation of State in 2+1 Flavor QCD at High Temperatures*, *Phys. Rev. D* **97** (2018) 014510 [[1710.05024](#)].
- [6] S. Borsanyi et al., *Calculation of the axion mass based on high-temperature lattice quantum chromodynamics*, *Nature* **539** (2016) 69 [[1606.07494](#)].
- [7] T. Appelquist and R.D. Pisarski, *High-Temperature Yang-Mills Theories and Three-Dimensional Quantum Chromodynamics*, *Phys. Rev. D* **23** (1981) 2305.
- [8] K. Kajantie, M. Laine, K. Rummukainen and Y. Schroder, *The Pressure of hot QCD up to $g_6 \ln(1/g)$* , *Phys. Rev. D* **67** (2003) 105008 [[hep-ph/0211321](#)].
- [9] J.O. Andersen, M. Strickland and N. Su, *Three-loop HTL gluon thermodynamics at intermediate coupling*, *JHEP* **08** (2010) 113 [[1005.1603](#)].
- [10] J.O. Andersen, L.E. Leganger, M. Strickland and N. Su, *Three-loop HTL QCD thermodynamics*, *JHEP* **08** (2011) 053 [[1103.2528](#)].
- [11] L. Giusti and M. Pepe, *Equation of state of the SU(3) Yang–Mills theory: A precise determination from a moving frame*, *Phys. Lett. B* **769** (2017) 385 [[1612.00265](#)].
- [12] M. Dalla Brida, L. Giusti, T. Harris, D. Laudicina and M. Pepe, *Non-perturbative thermal QCD at all temperatures: the case of mesonic screening masses*, *JHEP* **04** (2022) 034 [[2112.05427](#)].
- [13] L. Giusti, T. Harris, D. Laudicina, M. Pepe and P. Rescigno, *Baryonic screening masses in QCD at high temperature*, *Phys. Lett. B* **855** (2024) 138799 [[2405.04182](#)].
- [14] M. Bresciani, M.D. Brida, L. Giusti and M. Pepe, *The QCD Equation of State with $N_f = 3$ flavours up to the electro-weak scale*, [2501.11603](#).
- [15] L. Giusti and H.B. Meyer, *Implications of Poincare symmetry for thermal field theories in finite-volume*, *JHEP* **01** (2013) 140 [[1211.6669](#)].
- [16] M. Dalla Brida, L. Giusti and M. Pepe, *Non-perturbative definition of the QCD energy-momentum tensor on the lattice*, *JHEP* **04** (2020) 043 [[2002.06897](#)].

- [17] ALPHA collaboration, *Non-perturbative quark mass renormalisation and running in $N_f = 3$ QCD*, *Eur. Phys. J. C* **78** (2018) 387 [[1802.05243](#)].
- [18] ALPHA collaboration, *A non-perturbative exploration of the high energy regime in $N_f = 3$ QCD*, *Eur. Phys. J. C* **78** (2018) 372 [[1803.10230](#)].
- [19] ALPHA collaboration, *QCD Coupling from a Nonperturbative Determination of the Three-Flavor Λ Parameter*, *Phys. Rev. Lett.* **119** (2017) 102001 [[1706.03821](#)].
- [20] L. Giusti and M. Pepe, *Energy-momentum tensor on the lattice: Nonperturbative renormalization in Yang-Mills theory*, *Phys. Rev. D* **91** (2015) 114504 [[1503.07042](#)].
- [21] M. Bresciani, M. Dalla Brida, L. Giusti, M. Pepe and F. Rapuano, *Non-perturbative renormalization of the QCD flavour-singlet local vector current*, *Phys. Lett. B* **835** (2022) 137579 [[2203.14754](#)].
- [22] S.L. Adler, *Overrelaxation Algorithms for Lattice Field Theories*, *Phys. Rev. D* **37** (1988) 458.
- [23] N. Cabibbo and E. Marinari, *A New Method for Updating $SU(N)$ Matrices in Computer Simulations of Gauge Theories*, *Phys. Lett. B* **119** (1982) 387.
- [24] M. Bruno and R. Sommer, *On fits to correlated and auto-correlated data*, *Comput. Phys. Commun.* **285** (2023) 108643 [[2209.14188](#)].
- [25] F. Joswig, S. Kuberski, J.T. Kuhlmann and J. Neuendorf, *pyerrors: A python framework for error analysis of Monte Carlo data*, *Comput. Phys. Commun.* **288** (2023) 108750 [[2209.14371](#)].
- [26] A. Ramos, *Automatic differentiation for error analysis of Monte Carlo data*, *Comput. Phys. Commun.* **238** (2019) 19 [[1809.01289](#)].
- [27] N. Husung, P. Marquard and R. Sommer, *Asymptotic behavior of cutoff effects in Yang–Mills theory and in Wilson’s lattice QCD*, *Eur. Phys. J. C* **80** (2020) 200 [[1912.08498](#)].
- [28] N. Husung, P. Marquard and R. Sommer, *The asymptotic approach to the continuum of lattice QCD spectral observables*, *Phys. Lett. B* **829** (2022) 137069 [[2111.02347](#)].
- [29] N. Husung, *Logarithmic corrections to $O(a)$ and $O(a^2)$ effects in lattice QCD with Wilson or Ginsparg–Wilson quarks*, *Eur. Phys. J. C* **83** (2023) 142 [[2206.03536](#)].
- [30] P.A. Baikov, K.G. Chetyrkin and J.H. Kühn, *Five-Loop Running of the QCD coupling constant*, *Phys. Rev. Lett.* **118** (2017) 082002 [[1606.08659](#)].
- [31] M. Laine and Y. Schroder, *Quark mass thresholds in QCD thermodynamics*, *Phys. Rev. D* **73** (2006) 085009 [[hep-ph/0603048](#)].
- [32] L. Giusti and H.B. Meyer, *Thermal momentum distribution from path integrals with shifted boundary conditions*, *Phys. Rev. Lett.* **106** (2011) 131601 [[1011.2727](#)].

- [33] M. Bresciani, M. Dalla Brida, L. Giusti and M. Pepe, *Progresses on high-temperature QCD: Equation of State and energy-momentum tensor*, *PoS LATTICE2023* (2024) 192 [2312.11009].
- [34] S. Caracciolo, G. Curci, P. Menotti and A. Pelissetto, *The Energy Momentum Tensor for Lattice Gauge Theories*, *Annals Phys.* **197** (1990) 119.
- [35] S. Caracciolo, G. Curci, P. Menotti and A. Pelissetto, *Renormalization of the Energy Momentum Tensor and the Trace Anomaly in Lattice QED*, *Phys. Lett.* **B228** (1989) 375.
- [36] S. Caracciolo, P. Menotti and A. Pelissetto, *Analytic determination at one loop of the energy momentum tensor for lattice QCD*, *Phys. Lett.* **B260** (1991) 401.
- [37] S. Caracciolo, P. Menotti and A. Pelissetto, *One loop analytic computation of the energy momentum tensor for lattice gauge theories*, *Nucl. Phys.* **B375** (1992) 195.
- [38] H.B. Meyer, *Transport Properties of the Quark-Gluon Plasma: A Lattice QCD Perspective*, *Eur. Phys. J. A* **47** (2011) 86 [1104.3708].